THE JOURNAL OF PHYSICAL CHEMISTRY A

Article

pubs.acs.org/JPCA

Direct Determination of Resonance Energy Transfer in Photolyase: Structural Alignment for the Functional State

Chuang Tan,[†,§] Lijun Guo,[†,§] Yuejie Ai,[‡] Jiang Li,[†] Lijuan Wang,[†] Aziz Sancar,[∥] Yi Luo,[‡] and Dongping Zhong*[,†]

[†]Department of Physics, Department of Chemistry and Biochemistry, and Programs of Biophysics, Chemical Physics, and Biochemistry, The Ohio State University, 191 West Woodruff Avenue, Columbus, Ohio 43210, United States

[‡]Theoretical Chemistry, School of Biotechnology, Royal Institute of Technology, Roslagstullsbacken 15, SE-10691 Stockholm, Sweden

[∥]Department of Biochemistry and Biophysics, University of North Carolina School of Medicine, 120 Mason Farm Road, Chapel Hill, North Carolina 27599, United States

Supporting Information

ABSTRACT: Photoantenna is essential to energy transduction in photoinduced biological machinery. A photoenzyme, photolyase, has a light-harvesting pigment of methenyltetrahydrofolate (MTHF) that transfers its excitation energy to the catalytic flavin cofactor $FADH^-$ to enhance DNA-repair efficiency. Here we report our systematic characterization and direct determination of the ultrafast dynamics of resonance energy transfer from excited MTHF to three flavin redox states in *E. coli* photolyase by capturing the intermediates formed through the energy transfer and thus excluding the electron-transfer quenching pathway. We observed 170 ps for excitation energy transferring to the fully reduced hydroquinone $FADH^-$, 20 ps to the fully oxidized FAD, and 18 ps to the neutral semiquinone $FADH^•$, and the corresponding orientation factors (κ^2) were determined to be 2.84, 1.53 and 1.26, respectively, perfectly matching with our calculated theoretical values. Thus, under physiological conditions and over the course of evolution, photolyase has adopted the optimized orientation of its photopigment to efficiently convert solar energy for repair of damaged DNA.

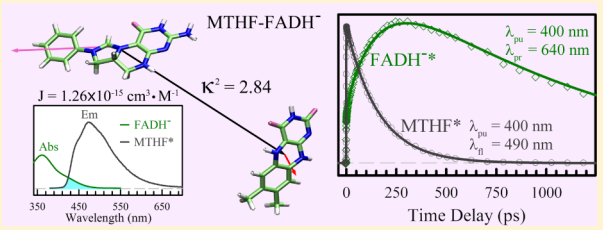

INTRODUCTION

Light harvesting by photoantenna is critical to photobiological machinery, and resonance energy transfer (RET) from antenna pigments is a vitally important means in energy transduction to convert solar energy into all kinds of biological processes such as in photosynthesis for charge separation to store chemical energy[1−4] and in xanthorhodopsin for retinal isomerization to induce proton transport.[5,6] The antenna pigments in photo-machinery have a wide range of absorption from UV to near-infrared and efficiently harvest energy to enhance biological functions especially under dim light. Various mechanistic models including coherent and noncoherent energy transfer have been recently proposed, especially in photosynthetic systems,[7−9] but the classic RET is still the most prevalent transfer way in nature.[10−12]

Photolyase, a light-driven enzyme machine, repairs UV-induced DNA damage using blue light as energy source. Photolyase contains two noncovalently bound chromophores: One is a fully reduced flavin adenine dinucleotide ($FADH^-$) as the catalytic cofactor to carry out the repair function upon excitation and the other one is either methenyltetrahydrofolate (MTHF) or 8-hydroxy-7,8-didemethyl-5-deazariboflavin (8-HDF) as an antenna pigment.[13] In *E. coli* photolyase, the flavin cofactor $FADH^-$ is deeply buried within the α-helical domain and has an unusual U-shaped conformation with the isoalloxazine ring and adenine moiety in close proximity, while the photoantenna MTHF is located in a shallow cleft between the α-helical and α/β domains and partially sticks out to the enzyme surface (Figure 1).[14] During DNA repair, the antenna MTHF absorbs a blue-light photon and transfers excitation energy to the distant catalytic cofactor $FADH^-$ to yield excited singlet-state $FADH^-$*, a key species to initiate the catalytic repair process.[15,16] The mechanism of energy transfer over 16.8 Å separation is of Förster type via a long-range dipole−dipole interaction between MTHF* and $FADH^-$.[17] Because MTHF has a much higher extinction coefficient than $FADH^-$, such energy transfer increases DNA-repair efficiency under dime light. After purification of the protein, the cofactor in vitro can exist in three redox states: the oxidized FAD, neutral semiquinone $FADH^•$, and fully reduced anionic hydroquinone $FADH^-$. Figure 2 shows their relative absorption spectra together with the absorption and emission spectra of the photoantenna MTHF. Clearly, all three states have the spectral

Special Issue: Current Topics in Photochemistry

Received: May 3, 2014
Revised: July 7, 2014
Published: July 8, 2014

   dx.doi.org/10.1021/jp504349b | J. Phys. Chem. A 2014, 118, 10522−10530

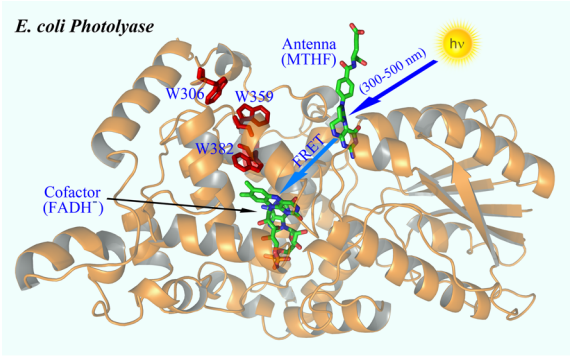

Figure 1. X-ray crystal structure of *E. coli* photolyase (orange ribbon) containing the photoantenna molecule (MTHF), the catalytic cofactor ($FADH^-$), and the conserved tryptophan triad (red stick) for photoreduction of the oxidized and neutral semiquinone flavin cofactor. FRET, Föster resonance energy transfer.

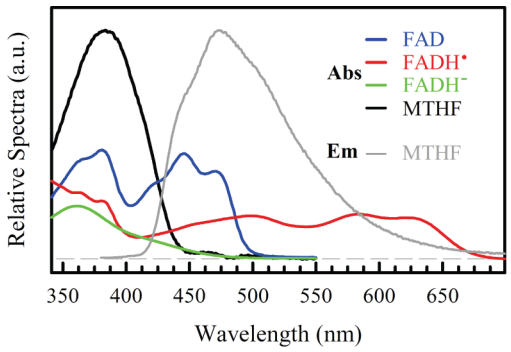

Figure 2. Steady-state spectra of *E. coli* photolyase. Shown are the relative absorption spectra (thick line) of the oxidized FAD (blue), neutral semiquinone $FADH^•$ (red), and anionic hydroquinone $FADH^-$ (green) and MTHF (black), and the emission spectrum of MTHF (thin gray line) of MTHF. The excitation wavelength for the MTHF emission was at 360 nm. The absorption spectrum was taken under anaerobic conditions for $FADH^-$, whereas the spectra were taken under aerobic conditions for FAD, $FADH^•$, and MTHF.

overlap of their absorption with the emission of MTHF*, leading to RET at a long distance. However, the catalytic cofactor $FADH^-$ has obviously the smallest spectral overlap integral and thus has the slowest transfer rate, but we have recently revealed that only $FADH^-$, not other redox states, is the active state for repair of damaged DNA.[18] Hence, the key question is what the structural alignments, that is, orientation factors (κ^2), are for the three redox states and whether the photoantenna has adopted the optimized structural configuration for the functional state $FADH^-$ over the course of evolution.

The energy transfer from MTHF* to $FADH^-$ and $FADH^•$ has been previously studied,[19,20] mainly by measuring the fluorescence quenching dynamics of MTHF*, but the excited flavin species after energy transfer has never been clearly observed, and thus the RET mechanism has not been directly established. Also, the MTHF* lifetime in photolyase without the energy acceptor, a key parameter in RET, has not been accurately determined. Here, with femtosecond spectroscopy and site-directed mutagenesis, we report our systematic studies of RET from MTHF* to the three flavin redox states of FAD, $FADH^•$, and $FADH^-$, respectively, by not only measuring the dynamics of MTHF* but also capturing the excited-state formation of the flavin species through RET. We also examine the subsequent dynamics of the excited three states at the active site after RET. With a single-position mutation of N341A at the active site, the flavin cofactor is released, but the binding site of MTHF is not affected. We can accurately determine the lifetime of MTHF* without any energy acceptor. Thus, with all measured RET dynamics and determined time scales, we finally evaluate the orientation factors for the three states and compare with our calculated theoretical values.

MATERIALS AND METHODS

Sample Preparation. The *E. coli* photolyase and the mutant N341A were prepared as previously described.[21,22] After purification, the flavin cofactor in the wild-type photolyase mostly exists in the neutral semiquinone $FADH^•$ state. To reduce the flavin cofactor to the hydroquinone $FADH^-$ state, we purged the protein with high-purity argon to remove oxygen and then illuminated it with a high-intensity lamp (150 W) under anaerobic conditions using a cutoff filter at 550 nm to ensure the protein exposed at >550 nm for photoreduction.[23] To obtain photolyase containing pure oxidized FAD,[24] we incubated the protein with semiquinone $FADH^•$ in a buffer of 50 mM Tris-HCl, 300 mM NaCl, 500 mM imidazole, and 10% (V/V) glycerol under pH 7.4 at 4 °C. The absorption spectra were monitored during oxidation. The absorption peaks of semiquinnone $FADH^•$ at 580 and 625 nm decrease and the peaks of oxidized FAD at 475, 450, and 425 nm increase. Until the semiquinone was completely depleted, the protein was applied to a Hi Trap Heparin HP column (5 mL) and eluted with a linear gradient of 0.2 to 1 M NaCl. The protein was dialyzed against the reaction buffer of 50 mM Tris-HCl, 100 mM NaCl, 1 mM EDTA, and 50% (v/v) glycerol under pH 7.4 and then stored at −80 °C.

Fluorescence Quantum Yield of Excited MTHF. Because of the lack of flavin cofactor, the mutant N341A was used to measure the fluorescence quantum yield (Φ_F) of MTHF* in photolyase. The most reliable method for measuring Φ_F is to use a well-characterized molecular system for a comparison.[25] The coumarin 1 in ethanol was selected as the standard with the known Φ_F value of 0.73 at the excitation wavelength of 360 nm.[26] A set of the standard and N341A samples with different concentrations were prepared. Both samples should be very dilute with the absorbance of <0.05 in a 5 mm quart cuvette to avoid any other artificial effects. The UV−vis absorption spectra and the fluorescence spectra excited at 360 nm of both the standard and N341A samples were recorded from the lower to relatively higher concentrations. Then, the integrated fluorescence intensities were plotted via the absorbance at 360 nm (Figure S1 in the Supporting Information). Because the standard and N341A samples with an identical absorbance can be assumed to absorb the same number of photons, the ratio of the slopes of the two plots is proportional to the ratio of their quantum yields of the two samples. With the known fluorescence quantum yield of the standard sample (Φ_{ST}), the quantum yield of N341A was calculated according to the following equation:

$$\Phi_X = \Phi_{ST}\left(\frac{\text{slope}_X}{\text{slope}_{ST}}\right)\left(\frac{n_X^2}{n_{ST}^2}\right) \quad (1)$$

where the subscripts ST and X denote the standard and N341A samples, respectively, and n is the refractive index of solution. The refractive index is 1.36 in ethanol and 1.39 in N341A

dx.doi.org/10.1021/jp504349b | J. Phys. Chem. A 2014, 118, 10522−10530

solution.[19] The experiments were repeated three times, and the fluorescence quantum yield of N341A is determined to be 0.408 after averaging three independent measurements of 0.407, 0.427, and 0.391.

Femtosecond-Resolved Spectroscopy. All femtosecond-resolved measurements were carried out using the fluorescence up-conversion and transient-absorption methods. The experimental laser layout and the procedure have been detailed elsewhere.[20,23] The excitation wavelength was set at 400 nm for all three redox states. The instrument response time is ~250 fs, and all the experiments were done at the magic angle (54.7°). All experiments used 5 mm quartz cuvettes (Starna), and the samples in cuvettes were kept stirring during irradiation to avoid heating and photobleaching. All femtosecond-resolved experiments were carried out under anaerobic conditions for the $FADH^-$ state and under aerobic conditions for FAD and $FADH^•$ states with a protein concentration of 200–400 μM. The fitting models of all transients are given in Figure S2 of the SI.

Theoretical Calculations. The conventional models for MTHF and flavin molecules are used for computational studies, as shown in Figure S3 in the Supporting Information. All structural optimizations of these models were carried out by density functional theory (DFT) with the hybrid functional B3LYP and a large basis set 6-311++G (2d, 2p). Transition dipole moments and excitation energies were then calculated on the optimized structures with time-dependent density functional theory (TDDFT) at the same computational level. To mimic the protein environment, we adopted a polarizable continuum model (IEF-PCM) in the equilibrium time regime in combination with a static dielectric constant of 4 throughout the calculations. All calculations were performed with the Gaussian 09 package.

RESULTS AND DISCUSSION

Ultrafast Fluorescence Dynamics and Quenching Time scales. Figure 3 shows the fluorescence dynamics of excited MTHF in the N341A mutant (Figure 3A) and in the wild-type photolyase with the three redox states (Figure 3B). All transients were gated around the emission peak at 480 or 490 nm and thus have the minimal contribution of the local protein relaxation,[27−30] reflecting the effective lifetime of the excited state. At 400 nm excitation, the absorption of MTHF is dominant due to its relatively higher absorption coefficient (Figure 2).[13] Even though part of flavin cofactors was excited, the fluorescence transients gated at 490 nm are from the MTHF* emission, and the emission from the flavin states is negligible: For FAD*, the excited state would be completely quenched by ultrafast electron transfer with neighboring aromatic residues in <1 ps;[24,31] for $FADH^•$*, the emission is ~700 nm, and no emission contribution is at 480 nm;[32] for $FADH^-$*, the weak emission has two peaks at 510 and 540 nm and the lifetime is ~1.3 ns.[23] Even considering the active-site solvation dynamics at the blue side of 490 nm, the transient[33] is completely different from that of MTHF*-$FADH^-$ in Figure 3B. Thus, the observed fluorescence dynamics of the three redox states in Figure 3B are completely from the excited MTHF, not from any excited flavin species.

In Figure 3A, we obtained a lifetime of 2.6 ns for MTHF* at the binding site without the energy acceptor of flavin cofactor, similar to that of 2.55 ns in *C. crescentus* photolyase[34] but much longer than 354 ps estimated from a reconstituted *E. coli* photolyase with a synthetic MTHF previously reported.[15,19,35]

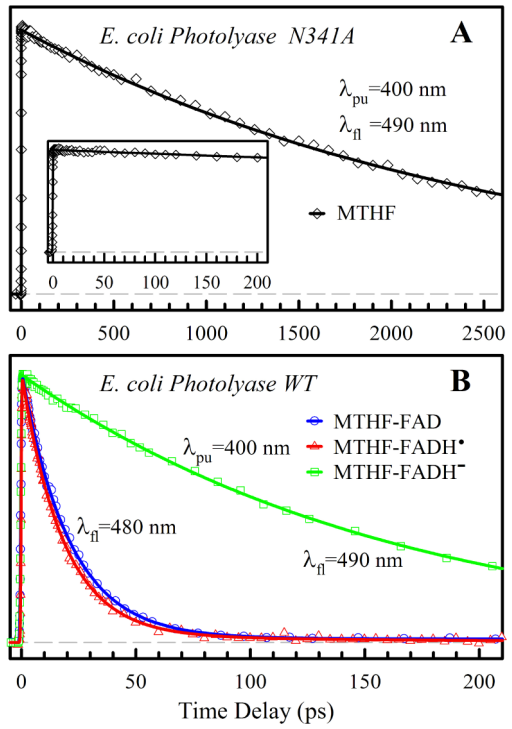

Figure 3. (A) Femtosecond-resolved fluorescence dynamics of MTHF* at the binding site of the mutant N341A gated at 490 nm. The short-range dynamics is shown in the inset with no ultrafast decay. (B) Femtosecond-resolved fluorescence quenching dynamics of MTHF*. The normalized fluorescence transients were measured for the complexes of MTHF-FAD (blue) and MTHF-$FADH^•$ (red) gated at 480 nm and of MTHF-$FADH^-$ (green) gated at 490 nm. All dynamics follow a single exponential decay.

In Figure 3B, the observed ultrafast quenching dynamics of MTHF* thus probably represent excitation energy transfer from MTHF* to the three flavin redox states. All transients are well-fitted by a single-exponential decay with the time constants of 160 ps for $FADH^-$, 20 ps for FAD, and 18 ps for $FADH^•$. We have recently measured the binding-site solvation of MTHF* and observed multiple solvation time scales of 4, 38, and 450 ps.[33] Thus, the observed RET processes in the three redox states in Figure 3B are coupled to the local protein relaxation, and the dynamics is in nonequilibrium. The dynamics would usually show a nonexponential behavior, either contracted or stretched, depending on the evolution of the spectral overlap due to the time-dependent emission spectra resulting from the local protein relaxation.[36] However, in the binding site of MTHF, we did not observe the significant emission peak shifts (Stokes shifts) instead of some spectral shape changes with time.[33] Thus, the spectral overlap is nearly invariant with time, leading to the observed single-exponential decay behavior. Taking into account the lifetime contribution (2.6 ns), we finally obtained the quenching time scales of possible RET dynamics of MTHF* in 170, 20, and 18 ps for $FADH^-$, FAD and $FADH^•$, respectively.

Capture of Flavin Intermediates and Determination of RET. *A. Anionic Hydroquinone State $FADH^-$.* To confirm that the fluorescence quenching of MTHF* is due to RET to the cofactor flavin, not electron transfer or other nonradiative processes, we need to detect the $FADH^-$* formation, an intermediate through RET from MTHF*. Figure 4 shows a series of absorption transients probed from 700 to 500 nm to

dx.doi.org/10.1021/jp504349b | J. Phys. Chem. A 2014, 118, 10522−10530

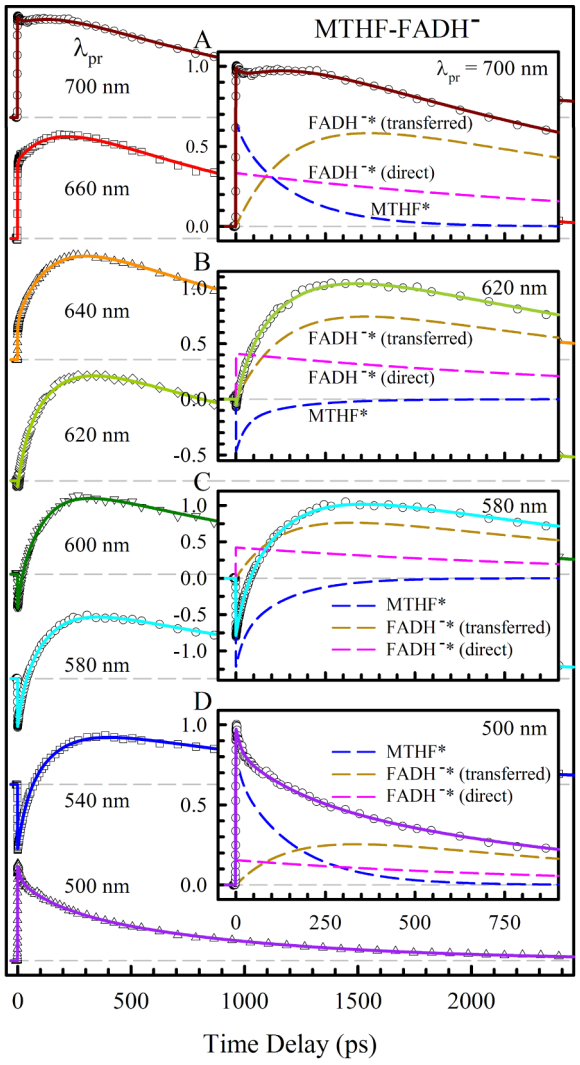

Figure 4. Femtosecond-resolved transient-absorption dynamics probed from 500 to 700 nm upon excitation at 400 nm. The transients can be systematically deconvoluted to three components (insets A–D) of the excited MTHF (dashed blue), the excited $FADH^-$ from RET of MTHF* (dashed dark goldenrod), and the directly excited $FADH^-$ (dashed pink). Note the distinct rise signals reflecting the intermediate formation through RET of MTHF*.

search for the $FADH^-$* formation by RET. Over the range of our probing wavelengths, only MTHF* and $FADH^-$* species have their absorption and exhibit transient signals. Strikingly, we observed a series of absorption transients with a distinct long rise-decay pattern at wavelengths longer than 500 nm (Figure 4A–C), especially the prominent rising signals probed from 540 to 660 nm. The long rising component unambiguously results from the intermediate, and thus we captured the $FADH^-$* formation by RET. All transients can be well fit by three components (Figure 4A–D): the decay of MTHF* absorption or stimulated emission (negative formation signals in Figure 4B,C) with a time constant of 160 ps determined from the fluorescence quenching dynamics, $FADH^-$* decay in 1.3 ns directly excited at the pump wavelength of 400 nm, and $FADH^-$* rise and decay formed through energy transfer of MTHF*. By the systematic fitting of all transients (see the SI), we obtained the formation time of $FADH^-$* in 170 ps, equal to the fluorescence quenching time of MTHF*. Thus, the quenching dynamics of MTHF* is caused by a fast RET to the cofactor $FADH^-$ and the RET time is 170 ps.

The purified *E. coli* photolyase typically contains only substoichiometric MTHF (20–50% of concentrations).[37−39] From the known absorption spectra of MTHF and $FADH^-$, we derived a ratio of MTHF to $FADH^-$ to be 0.31 in our $FADH^-$ sample. We also obtained this ratio from the derived direct and transferred $FADH^-$* concentrations by knowing the extinction coefficients of MTHF and $FADH^-$ at 400 nm, 21 675, and 2861 M^{-1} cm^{-1}, respectively. Thus, the direct $FADH^-$* signal in Figure 4 comes from two kinds of photolyase: One contains both chromophores of MTHF and $FADH^-$ (31%) and the other one has only the flavin cofactor $FADH^-$ (69%). The transferred $FADH^-$* signal is formed completely from RET of MTHF* in 170 ps, and this time is much faster than our previously reported value of 292 ps.[20] In that study, we also observed the same total quenching dynamics in 160 ps, but we used 354 ps as the MTHF* lifetime, obtained from the reconstituted photolyase with a synthetic MTHF that does not have the oligoglutamate side chain found in the native enzyme,[15,35] and seems to have a similar lifetime in solution (~300 ps)[19] rather than the actual lifetime of MTHF* (2.6 ns) bound in photolyase. Here, with a single-point mutation of N341A at the active site, the mutant photolyase releases the cofactor flavin but maintains the intact binding site of MTHF, and thus we acquired a true lifetime of MTHF* in 2.6 ns. With the determined new lifetime, the RET efficiency is ~94%, not 55% reported before.[20]

B. Oxidized State FAD. Figure 5 shows the absorption transients probed from 500 to 700 nm. Similarly, we observed a distinct rise in tens of picoseconds from 580 to 640 nm (also see Figure 5B,C), indicating an intermediate (FAD*) formation. Similar to the analyses above for the $FADH^-$ state, all signals are well fit by three parts: The first one represents the decay of MTHF* absorption or stimulated emission (negative formation signals in Figure 5B,C) with a time constant of 20 ps determined from the fluorescence quenching dynamics, the second signal results from the directly excited FAD* species at 400 nm, and the third part is related to the transferred FAD* from MTHF* with a distinct rise and decay pattern. It should be noted that the signal even from the directly excited FAD* at 400 nm in Figure 5 is complex and contains many components of different species. We have systematically characterized photoreduction of the oxidized FAD in *E. coli* photolyase without the chromophore MTHF and revealed multiple electron tunneling pathways to FAD*, especially with the conserved tryptophan triad (W382, W359, and W306 in Figure 1), and determined all electron-transfer dynamics and time scales.[24] For example, in Figure 5C of ref 24, we showed the absorption transient probed at 580 nm that was decomposed into five components from eight species with the reactant (FAD*), intermediates ($W382^+$, $W384^+$, $adenine^+$, $W316^+$, $W359^+$ and $W359^{\bullet}$.) and final product ($W306^+$). Thus, we completely followed the photoreduction dynamics of FAD[24] to simulate the signals from the directly excited FAD* and the decay dynamics of transferred FAD* in Figure 5. (See the SI.) We only need to fit the rise formation component of the transferred intermediate FAD* in 20 ps and all other dynamics of FAD* are completely the same as the dynamics of FAD photoreduction previously reported.[24]

By the systematic fitting of all transients (see the SI), we observed a ratio of 1:1 for the directly excited FAD* and transferred FAD*. Thus, both FAD* signals in Figure 5A–D

dx.doi.org/10.1021/jp504349b | J. Phys. Chem. A 2014, 118, 10522–10530

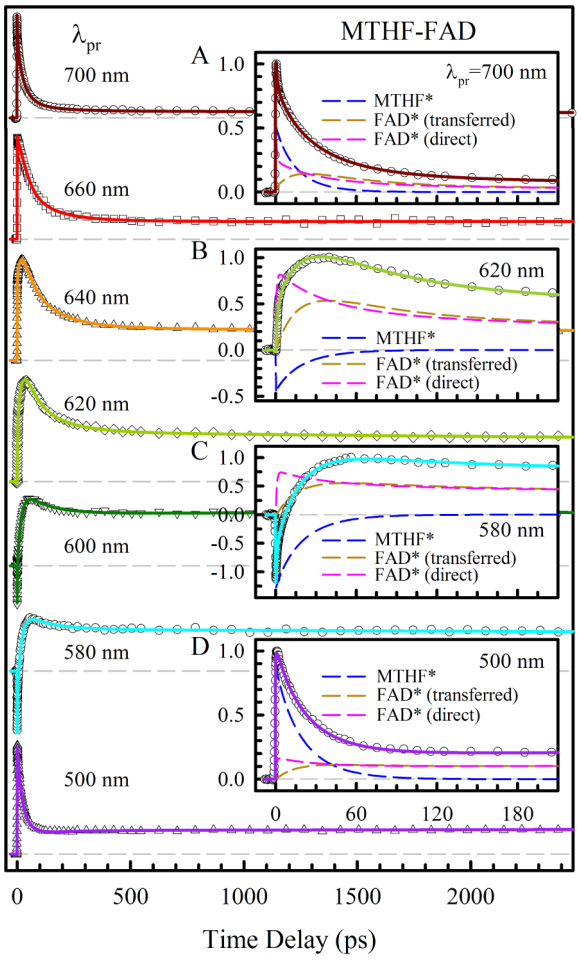

Figure 5. Femtosecond-resolved transient-absorption dynamics probed from 500 to 700 nm upon excitation at 400 nm. The transients can be systematically deconvoluted to three contributions (insets A–D) of the excited MTHF (dashed blue), the component resulting from the excited FAD from RET of MTHF* (dashed dark goldenrod), and the signal from the directly excited FAD (dashed pink). Note the distinct rise signals reflecting the intermediate formation through RET of MTHF* and the signal of the excited FAD containing its photoreduction dynamics; see the text.

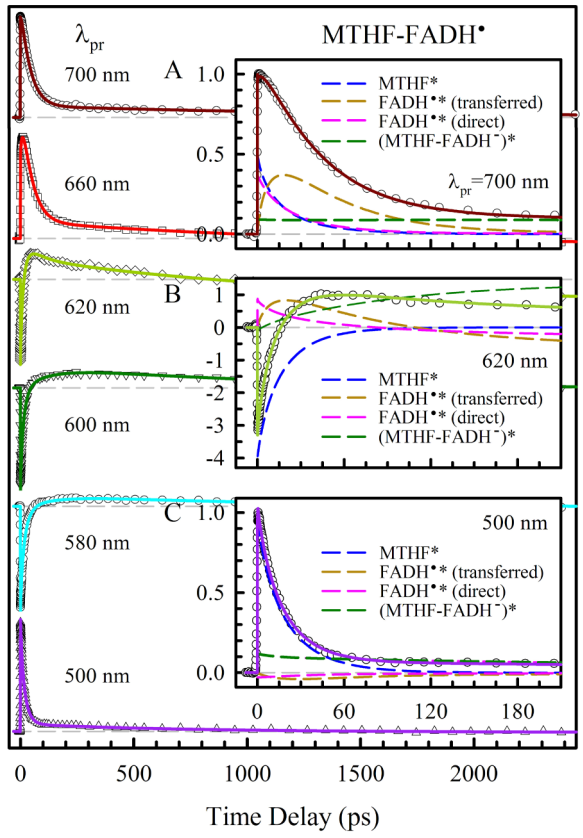

Figure 6. Femtosecond-resolved transient-absorption dynamics probed from 500 to 700 nm upon excitation at 400 nm. The transients can be systematically deconvoluted to four contributions (insets A–C) of the excited MTHF (dashed blue), the component resulting from the excited FADH• from RET of MTHF* (dashed dark goldenrod), the contribution from the directly excited FADH• (dashed pink), and a trace signal from the directly excited MTHF-FADH⁻ (dark green). Note the obvious rise signals around time zero reflecting the ultrafast intermediate formation through RET of MTHF* and the signal of the excited FADH• containing its photoreduction dynamics; see the text.

merge to the same values at a long time, that is, following the exactly same longtime behaviors. According to the extinction coefficients of FAD and MTHF at the pump wavelength of 400 nm, we derived a ratio of MTHF to FAD to be 0.27 in our FAD sample, similar to the ratio obtained from the absorption spectrum and slightly smaller than 0.31 of the $FADH^-$ sample above, probably due to the sample preparation. Thus, given the lifetime of MTHF* in 2.6 ns, the RET in 20 ps is ultrafast and leads to an extremely high energy-transfer quantum yield of 0.992.

C. Neutral Semiquinone State FADH•. Figure 6 shows the absorption transients probed at 500 to 700 nm. Similarly, the transients at the wavelengths longer than 620 nm show a clear rise signal of ~20 ps, especially a bump around time zero indicating a rise component, as shown in Figure 6A at 700 nm. Similar to the FAD state, we as well as others have recently carried out the systematic characterization of FADH• photoreduction and revealed all various electron-transfer (ET) dynamics.[20,40−43] We did not observe a positive rise signal in those transients with a rise time ~20 ps in photoreduction.[41]

Therefore, the rising signal has to come from the formation of the intermediate FADH•* through RET from MTHF*, and thus we observed the product formation by RET from MTHF*. For all transients, we here have to fit four parts: One component is from the MTHF* decay dynamics in 18 ps determined from the fluorescence quenching dynamics; the second signal is from FADH•* directly excited at 400 nm and following a FADH•* photoreduction behavior;[41] the third component is from the transferred FADH•* from MTHF* through RET with a rise and then decay that again follows the FADH* photoreduction dynamics; finally, the fourth component that we have to fit is from the (MTHF-$FADH^-$)* species with a total amplitude of ~5%. This signal is due to FADH•* photoreduction to $FADH^-$, and the $FADH^-$ has not completely oxidized to FADH• in 2 ms with next laser pulse excitation (the pump laser repetition rate is at 500 Hz); that is, in the protein sample, there is a trace of the sample with the $FADH^-$ state. By the systematic fitting of all the transients (see the SI), we obtained the rise formation time in 18 ps, consistent with the RET time from MTHF* determined by the fluorescence dynamics. Similar to the FAD state, the photoreduction signal from FADH•* is complex and has many contributions of various species. (See the SI for data analysis.)[41] With knowing

dx.doi.org/10.1021/jp504349b | J. Phys. Chem. A 2014, 118, 10522−10530

the extinction coefficients of MTHF and FADH$^{\bullet}$ at 400 nm and the fitted ratio of directly excited to transferred FADH$^{\bullet}$, we derived a ratio of MTHF to FADH$^{\bullet}$ to be 0.31 in our FADH$^{\bullet}$ sample, as calculated from the absorption spectrum. The observed RET in 18 ps in FADH$^{\bullet}$ state is ultrafast, also resulting in an extremely high energy-transfer quantum yield of 0.993, similar to the efficiency for the FAD state.

Evaluation of Orientation Factors and Optimization of Structural Alignments. According to the classic Föster resonance energy transfer theory, the long-range FRET rate (k_{RET}) from MTHF* to the flavin cofactor depends on the relative position (r) and orientations of donor (MTHF) and acceptor (flavin) and can be expressed as follows[10]

$$k_{RET} = \frac{1}{\tau_D}\left(\frac{R_0}{r}\right)^6 \tag{2}$$

$$R_0 = 9.78 \times 10^2(\kappa^2 n^{-4} Q_D J)^{1/6} \tag{3}$$

where R_0, the Föster distance, is defined as the donor−acceptor distance in angstroms, at which the transfer efficiency is 50%. Q_D and τ_D are the donor's fluorescence quantum yield and lifetime in the absence of acceptor, respectively, r is the center-to-center distance between the donor and acceptor in angstroms, κ^2 is the orientation factor, n is the refractive index of the medium (1.39),[19] and J is the spectral overlap integral between the donor's emission and acceptor's absorption in unit of cm^3 M^{-1}. The X-ray structure reported a distance (r) of 16.8 Å between MTHF and the flavin cofactor.[14] Given the FRET rates from MTHF to the three flavin states and the lifetime of MTHF* (τ_D = 2.6 ns), the derived values of R_0 are 37.81 Å for MTHF*-FAD, 38.48 Å for MTHF*-FADH$^{\bullet}$, and 26.47 Å for MTHF*-FADH$^-$. The spectral overlap integral is generally expressed as follows[10]

$$J = \frac{\int F(\lambda)\varepsilon(\lambda)\lambda^4\, d\lambda}{\int F(\lambda)\, d\lambda} \tag{4}$$

where $F(\lambda)$ represents the emission spectrum of the donor in the absence of the acceptor and $\varepsilon(\lambda)$ is the absorbance molar extinction coefficients of the acceptor in units of cm^{-1}·M^{-1}. Because we did not observe an significant change of the emission spectra with time,[33] we can consider the J value to be a time-independent constant.[36] Typically, the steady-state fluorescence and absorption spectra (Figures 2 and 7) are used to calculate the J values. The derived three J values for the three flavin redox states are listed in Table 1 and Figure 7. From the N341A mutant, we obtained a fluorescence quantum yield of 0.408 for MTHF*. (See the SI.) Using eq 2, we derived the orientation factors (κ^2) for the three states of FAD, FADH$^{\bullet}$, and FADH$^-$ to be 1.53, 1.26, and 2.84, respectively. We previously reported smaller orientation factors[20] of 0.28 and 0.11 for FADH$^{\bullet}$ and FADH$^-$, respectively, mainly due to the use of a short lifetime of MTHF* (τ_D) of 354 ps in calculation,[19] leading to the smaller R_0 values. With the precise determination of the MTHF* lifetime (τ_D) and fluorescence quantum yield (Q_D) in the intact binding site, the current values are much reliable and accurate. All three values are larger than a statistic average of 2/3, indicating that for RET in proteins the orientation factors have a specific value and are usually not equal to 2/3, as we also reported RET in myoglobin.[36,44] Significantly, we observed an unusual large orientation factor of 2.84 for the functional state FADH$^-$, the largest among all three states, indicating the protein over the course of evolution has evolved to an optimized structural configuration of MTHF toward the active-state FADH$^-$ to maximize the energy transfer for photolyase function. Also, it further confirms the FADH$^-$ as the functional state.

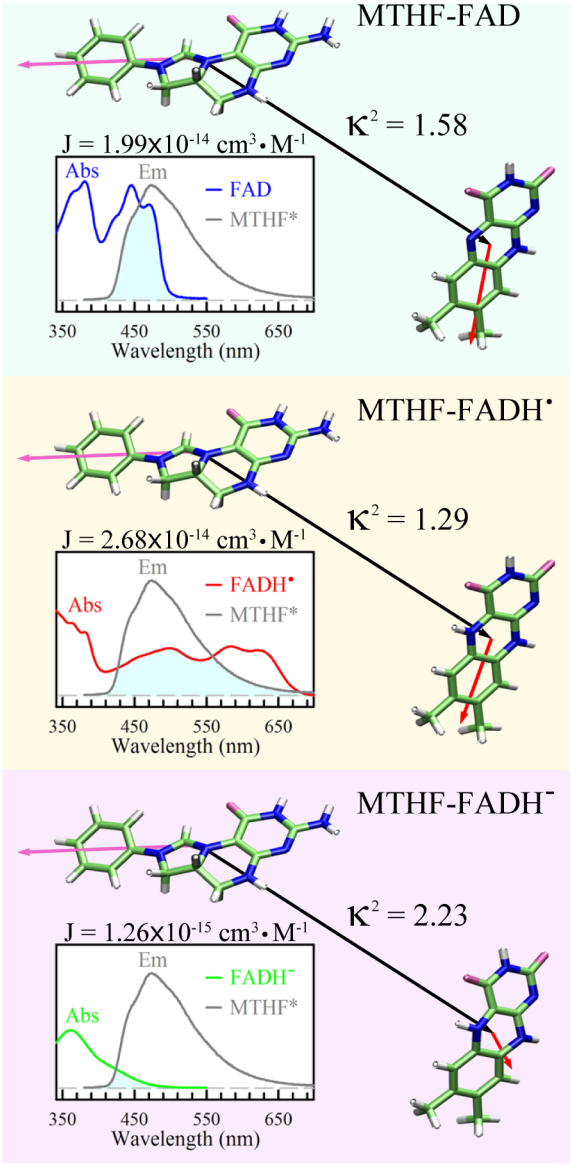

Figure 7. Theoretical calculations of the orientation factors and spectral overlap integrals of the complexes of MTHF with three flavin redox states. Shown are the optimized structures of three donor−acceptor pairs of MTHF-FAD, MTHF-FADH$^{\bullet}$, and MTHF-FADH$^-$. These three configurations in the panels were aligned with MTHF. The orientation factors (κ^2) were calculated by three unit vectors of the mass center-to-center of the donor and acceptor (black arrow) and the calculated transition dipole moments of MTHF (pink arrow) and flavin cofactors (red arrow). The insets show the spectra overlaps between the emission of MTHF and the absorption of three flavin cofactors.

To confirm such important finding, we also performed the theoretical studies to evaluate the orientation factors. Using the initial configuration from the X-ray structure of *E. coli* DNA photolyase for the MTHF-flavin pair, the optimized structures and transition dipole moments were obtained and the κ^2 values were estimated through the following equation[10]

dx.doi.org/10.1021/jp504349b | J. Phys. Chem. A 2014, 118, 10522−10530

Table 1. Derived Orientation Factors (κ^2) from Both Experimental and Theoretical Studies

MTHF-	τ_{FRET} (ps)	τ_D (ps)[a]	(R_0^6/r^6)[b]	r (Å)[c]	R_0 (Å)	Q_D	n	J ($cm^3 \cdot M^{-1}$)	κ^2 (exptl.)	κ^2 (theor.)
FAD	20	2600	130.00	16.8	37.81	0.408	1.39	1.99×10^{-14}	1.53	1.58
$FADH^{\bullet}$	18	2600	144.44	16.8	38.48	0.408	1.39	2.68×10^{-14}	1.26	1.29
$FADH^-$	170	2600	15.29	16.8	26.47	0.408	1.39	1.26×10^{-15}	2.84	2.23

[a] τ_D is the lifetime of the donor MTHF in photolyase without any energy acceptor. [b] $(R_0/r)^6$ is calculated by τ_D/τ_{FRET}. [c] Distance of 16.8 Å (r) between MTHF and the flavin cofactor is from ref 14.

$$\kappa^2 = (\cos\theta_T - 3\cos\theta_D \cos\theta_A)^2 \quad (5)$$

where θ_T is the angle between the emission transition dipole of the donor and the absorption transition dipole of the acceptor and θ_D and θ_A are the angles between these dipoles and the vector joining the centers of the donor and acceptor. Figure 7 shows all of these vector directions for the optimized structures. The center-to-center vectors were found to be (−3.76, 9.71, 12.91) for MTHF-FAD, (−3.77, 9.71, 12.92) for MTHF-$FADH^{\bullet}$, and (−3.79, 9.70, 12.96) for MTHF-$FADH^-$. On the basis of the optimized structures, the transition dipoles were calculated using TDDFT. The emission transition dipole of MTHF is (2.39, −1.06, −1.16), and the absorption transition dipoles of the three states are (1.37, 0.34, 1.23), (1.25, 0.097, 1.05), and (0.14, 0.23, 0.18) for FAD, $FADH^{\bullet}$, and $FADH^-$, respectively, as shown in Figure 7. The isoalloxazine rings of FAD and $FADH^{\bullet}$ are nearly planar, and their transition dipole moments are in the flavin plane and with the angles of 77.6 and 84.9° relative to the N5−N10 axis, respectively, consistent with the previous reports.[45−47] In contrast, the flavin ring of the fully reduced $FADH^-$ is in a slight bent configuration that has been reported by MNR studies and various theoretical calculations.[48−52] The transition dipole moment of $FADH^-$ lies closer to the N5−N10 axis with an angle of 41.1°. With the directions of these transition dipoles and the center-to-center vectors, the orientation factors were determined to be 1.58 for MTHF-FAD, 1.29 for MTHF-$FADH^{\bullet}$, and 2.23 for MTHF-$FADH^-$. A similar system of *A. nidulans* photolyase for RET between the photoantenna 8-HDF and the functional state $FADH^-$ was found to have a large orientation factor of 1.82 by a theoretical calculation[53] and of 1.6 by an estimation from the X-ray structure.[54] It is striking that the experimentally derived orientation factors for FAD (1.53) and $FADH^{\bullet}$ (1.26) perfectly agree with the theoretical values of 1.58 and 1.29. For the functional state $FADH^-$, the experimental value of 2.84 is slightly larger than the theoretical prediction of 2.23 but in the right trend. The difference probably comes from the difficult calculation of an anionic excited state for a large-size flavin molecule. Overall, the theoretical calculations are perfectly consistent with the experimental observation and the enzyme has the optimized structural alignment for the RET pair of photoantenna MTHF and the functional state $FADH^-$ for efficient conversion of solar energy to perform the repair of damaged DNA.

CONCLUSIONS

We reported here our systematic characterization and analyses of RET from excited photoantenna (MTHF*) to three flavin redox states of the oxidized FAD, semiquinone $FADH^{\bullet}$ and fully reduced hydroquinone $FADH^-$ in *E. coli* photolyase. With femtosecond-resolved fluorescence and transient-absorption spectroscopic methods, we not only measured the initial reactant (MTHF*) quenching dynamics but, more importantly, also captured the intermediates by detection of the formation dynamics through energy transfer from the photoantenna and thus unambiguously determined the RET mechanism between the photoantenna and the catalytic cofactor in photolyase. We observed the energy transfer from the photoantenna to the fully reduced hydroquinone $FADH^-$ in 170 ps, to the semiquinone in 18 ps, and to the oxidized FAD in 20 ps. With a single-point mutation of N341A, we characterized intact photophysics of the photoantenna (MTHF) at the binding site in photolyase. With all results, we finally determined the orientation factors of these three energy-transfer pairs, 2.84, 1.26, and 1.53, for the hydroquinone, semiquinone, and oxidized states, respectively, perfectly consistent with our calculated theoretical values of 2.23, 1.29, and 1.57. This observation clearly shows that over the course of evolution photolyase has evolved to an optimized structural configuration between the photoantenna and the functional state with an unusual large orientation factor to maximize the energy transfer to perform the biological function of repair of damaged DNA and further confirmed that the anionic hydroquinone $FADH^-$ is only the active state in photolyase.[18]

ASSOCIATED CONTENT

Supporting Information

Analysis of fluorescence quantum-yield measurement, kinetic schemes of RET in three redox states, and computational models for MTHF and flavin molecules. This material is available free of charge via the Internet at http://pubs.acs.org.

AUTHOR INFORMATION

Corresponding Author

*E-mail: zhong.28@osu.edu. Tel: (614)-292-3044.

Author Contributions

[§]C.T. and L.G. contributed equally.

Notes

The authors declare no competing financial interest.

ACKNOWLEDGMENTS

We thank Dr. Ya-Ting Kao for the initial help with experiment. This work is supported in part by the National Institutes of Health (Grant GM074813), the National Science Foundation (Grant CHE0748358), the Camille Dreyfus Teacher-Scholar and the Guggenheim fellowship (to D.Z.), and the Ohio State University Pelotonia fellowship (to C.T. and J.L.).

REFERENCES

(1) Duysens, L. N. M. Photosynthesis. *Prog. Biophys. Mol. Biol.* **1964**, *14*, 1−104.

(2) Blankenship, R. E. *Molecular Mechanisms of Photosynthesis*; Blackwell Science: Malden, MA, 2002.

(3) Fleming, G. R.; van Grondelle, R. Femtosecond Spectroscopy of Photosynthetic Light-Harvesting Systems. *Curr. Opin. Struct. Biol.* **1997**, *7*, 738−748.

(4) Scholes, G. D.; Fleming, G. R.; Olaya-Castro, A.; van Grondelle, R. Lessons from Nature about Solar Light Harvesting. *Nat. Chem.* **2011**, *3*, 763−774.
(5) Balashov, S. P.; Imasheva, E. S.; Boichenko, V. A.; Anton, J.; Wang, J. M.; Lanyi, J. K. Xanthorhodopsin: A Proton Pump with a Light-Harvesting Carotenoid Antenna. *Science* **2005**, *309*, 2061−2064.
(6) Balashov, S. P.; Imasheva, E. S.; Wang, J. M.; Lanyi, J. K. Excitation Energy-Transfer and the Relative Orientation of Retinal and Carotenoid in Xanthorhodopsin. *Biophys. J.* **2008**, *95*, 2402−2414.
(7) Engel, G. S.; Calhoun, T. R.; Read, E. L.; Ahn, T. K.; Mancal, T.; Cheng, Y. C.; Blankenship, R. E.; Fleming, G. R. Evidence for Wavelike Energy Transfer through Quantum Coherence in Photosynthetic Systems. *Nature* **2007**, *446*, 782−786.
(8) Lee, H.; Cheng, Y. C.; Fleming, G. R. Coherence Dynamics in Photosynthesis: Protein Protection of Excitonic Coherence. *Science* **2007**, *316*, 1462−1465.
(9) Collini, E.; Wong, C. Y.; Wilk, K. E.; Curmi, P. M. G.; Brumer, P.; Scholes, G. D. Coherently Wired Light-Harvesting in Photosynthetic Marine Algae at Ambient Temperature. *Nature* **2010**, *463*, 644−647.
(10) Andrews, D. L.; Demidov, A. A. *Resonance Energy Transfer*; John Wiley & Sons: Chichester, England, 1999.
(11) Scholes, G. D. Long-Range Resonance Energy Transfer in Molecular Systems. *Annu. Rev. Phys. Chem.* **2003**, *54*, 57−87.
(12) Speiser, S. Photophysics and Mechanisms of Intramolecular Electronic Energy Transfer in Bichromophoric Molecular Systems: Solution and Supersonic Jet Studies. *Chem. Rev.* **1996**, *96*, 1953−1976.
(13) Sancar, A. Structure and Function of DNA Photolyase and Cryptochrome Blue-Light Photoreceptors. *Chem. Rev.* **2003**, *103*, 2203−2237.
(14) Park, H. W.; Kim, S. T.; Sancar, A.; Deisenhofer, J. Crystal Structure of DNA Photolyase from *Escherichia coli*. *Science* **1995**, *268*, 1866−1872.
(15) Payne, G.; Sancar, A. Absolute Action Spectrum of E-$FADH_2$ and E-$FADH_2$-MTHF Forms of *Escherichia coli* DNA Photolyase. *Biochemistry* **1990**, *29*, 7715−7727.
(16) Lipman, R. S. A.; Jorns, M. S. Direct Evidence for Singlet-Singlet Energy Transfer in *Escherichia coli* DNA Photolyase. *Biochemistry* **1992**, *31*, 786−791.
(17) Weber, S. Light-Driven Enzymatic Catalysis of DNA Repair: A Review of Recent Biophysical Studies on Photolyase. *Biochim. Biophys. Acta, Bioenerg.* **2005**, *1707*, 1−23.
(18) Liu, Z.; Zhang, M.; Guo, X.; Tan, C.; Li, J.; Wang, L.; Sancar, A.; Zhong, D. Dynamic Determination of the Functional State in Photolyase and the Implication for Cryptochrome. *Proc. Natl. Acad. Sci. U.S.A.* **2013**, *110*, 12972−12977.
(19) Kim, S. T.; Heelis, P. F.; Okamura, T.; Hirata, Y.; Mataga, N.; Sancar, A. Determination of Rates and Yields of Interchromophore (Folate→Flavin) Energy Transfer and Intermolecular (Flavin→DNA) Electron Transfer in *Escherichia coli* Photolyase by Time-Resolved Fluorescence and Absorption Spectroscopy. *Biochemistry* **1991**, *30*, 11262−11270.
(20) Saxena, C.; Sancar, A.; Zhong, D. Femtosecond Dynamics of DNA Photolyase: Energy Transfer of Antenna Initiation and Electron Transfer of Cofactor Reduction. *J. Phys. Chem. B* **2004**, *108*, 18026−18033.
(21) Sancar, A.; Smith, F. W.; Sancar, G. B. Purification of *Escherichia coli* DNA Photolyase. *J. Biol. Chem.* **1984**, *259*, 6028−6032.
(22) Liu, Z.; Tan, C.; Guo, X.; Kao, Y.-T.; Li, J.; Wang, L.; Sancar, A.; Zhong, D. Dynamics and Mechanism of Cyclobutane Pyrimidine Dimer Repair by DNA Photolyase. *Proc. Natl. Acad. Sci. U.S.A.* **2011**, *108*, 14831−14836.
(23) Kao, Y.-T.; Saxena, C.; Wang, L.; Sancar, A.; Zhong, D. Direct Observation of Thymine Dimer Repair in DNA by Photolyase. *Proc. Natl. Acad. Sci. U.S.A.* **2005**, *102*, 16128−16132.
(24) Liu, Z.; Tan, C.; Guo, X.; Li, J.; Wang, L.; Sancar, A.; Zhong, D. Determining Complete Electron Flow in the Cofactor Photoreduction of Oxidized Photolyase. *Proc. Natl. Acad. Sci. U.S.A.* **2013**, *110*, 12966−12971.
(25) Williams, A. T. R.; Winfield, S. A.; Miller, J. N. Relative Fluorescence Quantum Yields Using a Computer-Controlled Luminescence Spectrometer. *Analyst* **1983**, *108*, 1067−1071.
(26) Jones, G.; Jackson, W. R.; Choi, C.; Bergmark, W. R. Solvent Effects on Emission Yield and Lifetime for Coumarin Laser-Dyes. Requirements for a Rotatory Decay Mechanism. *J. Phys. Chem.* **1985**, *89*, 294−300.
(27) Lu, W.; Kim, J.; Qiu, W.; Zhong, D. Femtosecond Studies of Tryptophan Solvation: Correlation Function and Water Dynamics at Lipid Surfaces. *Chem. Phys. Lett.* **2004**, *388*, 120−126.
(28) Zhang, L.; Wang, L.; Kao, Y.-T.; Qiu, W.; Yang, Y.; Okobiah, O.; Zhong, D. Mapping Hydration Dynamics around a Protein Surface. *Proc. Natl. Acad. Sci. U.S.A.* **2007**, *104*, 18461−18466.
(29) Zhang, L.; Yang, Y.; Kao, Y.-T.; Wang, L.; Zhong, D. Protein Hydration Dynamics and Molecular Mechanism of Coupled Water-Protein Fluctuations. *J. Am. Chem. Soc.* **2009**, *131*, 10677−10691.
(30) Qin, Y.; Chang, C.-W.; Wang, L.; Zhong, D. Validation of Response Function Construction and Probing Heterogeneous Protein Hydration by Intrinsic Tryptophan. *J. Phys. Chem. B* **2012**, *116*, 13320−13330.
(31) Kao, Y.-T.; Tan, C.; Song, S. H.; Ozturk, N.; Li, J.; Wang, L.; Sancar, A.; Zhong, D. Ultrafast Dynamics and Anionic Active States of the Flavin Cofactor in Cryptochrome and Photolyase. *J. Am. Chem. Soc.* **2008**, *130*, 7695−7701.
(32) Kao, Y.-T.; Saxena, C.; He, T.-F.; Guo, L.; Wang, L.; Sancar, A.; Zhong, D. Ultrafast Dynamics of Flavins in Five Redox States. *J. Am. Chem. Soc.* **2008**, *130*, 13132−13139.
(33) Chang, C.-W.; et al. Ultrafast Solvation Dynamics at Binding and Active Sites of Photolyases. *Proc. Natl. Acad. Sci. U.S.A.* **2010**, *107*, 2914−2919.
(34) Ozturk, N.; Kao, Y.-T.; Selby, C. P.; Kavakli, I. H.; Partch, C. L.; Zhong, D.; Sancar, A. Purification and Characterization of a Type III Photolyase from *Caulobacter crescentus*. *Biochemistry* **2008**, *47*, 10255−10261.
(35) Johnson, J. L.; Hamm-Alvarez, S.; Payne, G.; Sancar, G. B.; Rajagopalan, K. V.; Sancar, A. Identification of the Second Chromophore of *Escherichia coli* and Yeast DNA Photolyases as 5,10-Methenyltetrahydrofolate. *Proc. Natl. Acad. Sci. U.S.A.* **1988**, *85*, 2046−2050.
(36) Stevens, J. A.; Link, J. J.; Zang, C.; Wang, L.; Zhong, D. Ultrafast Dynamics of Nonequilibrium Resonance Energy Transfer and Probing Globular Protein Flexibility of Myoglobin. *J. Phys. Chem. A* **2012**, *116*, 2610−2619.
(37) Hamm-Alvarez, S.; Sancar, A.; Rajagopalan, K. V. Role of Enzyme-Bound 5,10-Methenyltetrahydropteroylpolyglutamate in Catalysis by *Escherichia coli* DNA Photolyase. *J. Biol. Chem.* **1989**, *264*, 9649−9656.
(38) Hamm-Alvarez, S.; Sancar, A.; Rajagopalan, K. V. The Folate Cofactor of *Escherichia coli* DNA Photolyase Acts Catalytically. *J. Biol. Chem.* **1990**, *265*, 18656−18662.
(39) Hamm-Alvarez, S. F.; Sancar, A.; Rajagopalan, K. V. The Presence and Distribution of Reduced Folates in *Escherichia coli* Dihydrofolate Reductase Mutants. *J. Biol. Chem.* **1990**, *265*, 9850−9856.
(40) Wang, H.; Saxena, C.; Quan, D.; Sancar, A.; Zhong, D. Femtosecond Dynamics of Flavin Cofactor in DNA Photolyase: Radical Reduction, Local Solvation, and Charge Recombination. *J. Phys. Chem. B* **2005**, *109*, 1329−1333.
(41) Liu, Z.; Tan, C.; Guo, X.; Li, J.; Wang, L.; Zhong, D. Dynamic Determination of Active-Site Reactivity in Semiquinone Photolyase by the Cofactor Photoreduction. *J. Phys. Chem. Lett.* **2014**, *5*, 820−825.
(42) Aubert, C.; Vos, M. H.; Mathis, P.; Eker, A. P. M.; Brettel, K. Intraprotein Radical Transfer during Photoactivation of DNA Photolyase. *Nature* **2000**, *405*, 586−590.
(43) Byrdin, M.; Lukacs, A.; Thiagarajan, V.; Eker, A. P. M.; Brettel, K.; Vos, M. H. Quantum Yield Measurements of Short-Lived Photoactivation Intermediates in DNA Photolyase: Toward a Detailed Understanding of the Triple Tryptophan Electron Transfer Chain. *J. Phys. Chem. A* **2010**, *114*, 3207−3214.

(44) Stevens, J. A.; Link, J. J.; Kao, Y.-T.; Zang, C.; Wang, L.; Zhong, D. Ultrafast Dynamics of Resonance Energy Transfer in Myoglobin: Probing Local Conformation Fluctuations. *J. Phys. Chem. B* **2010**, *114*, 1498−1505.
(45) Eaton, W. A.; Hofrichter, J.; Makinen, M. W.; Andersen, R. D.; Ludwig, M. L. Optical Spectra and Electronic Structure of Flavine Mononucleotide in Flavodoxin Crystals. *Biochemistry* **1975**, *14*, 2146−2151.
(46) Johansson, L. B. A.; Davidsson, A.; Lindblom, G.; Naqvi, K. R. Electronic Transitions in the Isoalloxazine Ring and Orientation of Flavins in Model Membranes Studied by Polarized Light Spectroscopy. *Biochemistry* **1979**, *18*, 4249−4253.
(47) Matsuoka, Y.; Norden, B. Linear Dichroism Studies of Nucleic-Acids III. Reduced Dichroism Curves of DNA in Ethanol-Water and in Poly(vinyl alcohol) Films. *Biopolymers* **1983**, *22*, 1731−1746.
(48) Moonen, C. T. W.; Vervoort, J.; Muller, F. Reinvestigation of the Structure of Oxidized and Reduced Flavin: Carbon-13 and Nitrogen-15 Nuclear Magnetic Resonance Study. *Biochemistry* **1984**, *23*, 4859−4867.
(49) Moonen, C. T. W.; Vervoort, J.; Muller, F. Carbon-13 Nuclear Magnetic-Resonance Study on the Dynamics of the Conformation of Reduced Flavin. *Biochemistry* **1984**, *23*, 4868−4872.
(50) Dixon, D. A.; Lindner, D. L.; Branchaud, B.; Lipscomb, W. N. Conformations and Electronic-Structures of Oxidized and Reduced Isoalloxazine. *Biochemistry* **1979**, *18*, 5770−5775.
(51) Zheng, Y. J.; Ornstein, R. L. A Theoretical Study of the Structures of Flavin in Different Oxidation and Protonation States. *J. Am. Chem. Soc.* **1996**, *118*, 9402−9408.
(52) Choe, Y. K.; Nagase, S.; Nishimoto, K. Theoretical Study of the Electronic Spectra of Oxidized and Reduced States of Lumiflavin and its Derivative. *J. Comput. Chem.* **2007**, *28*, 727−739.
(53) Zheng, X. H.; Garcia, J.; Stuchebrukhov, A. A. Theoretical Study of Excitation Energy Transfer in DNA Photolyase. *J. Phys. Chem. B* **2008**, *112*, 8724−8729.
(54) Tamada, T.; Kitadokoro, K.; Higuchi, Y.; Inaka, K.; Yasui, A.; deRuiter, P. E.; Eker, A. P. M.; Miki, K. Crystal Structure of DNA Photolyase from *Anacystis nidulans*. *Nat. Struct. Biol.* **1997**, *4*, 887−891.